Supporting information for:

A dual-site approach in high-entropy oxide aerogels creates active and selective reverse water–gas shift catalysts

Travis G. Novak,*[a] Matthew R. Buck,[b] Austin E. Herzog,[c] Joshua J. Kim,[b] Bethany M. Hudak,[a] Ryan H. DeBlock,[a] Evan R. Glaser,[a] Michelle D. Johannes,[a] Debra R. Rolison*[a]

a. U.S. Naval Research Laboratory, Washington, DC 20375, USA

b. Chemistry Department, United States Naval Academy, Annapolis, MD 21402, USA

c. NRC Postdoctoral Associate, U.S. Naval Research Laboratory, Washington, DC 20375, USA

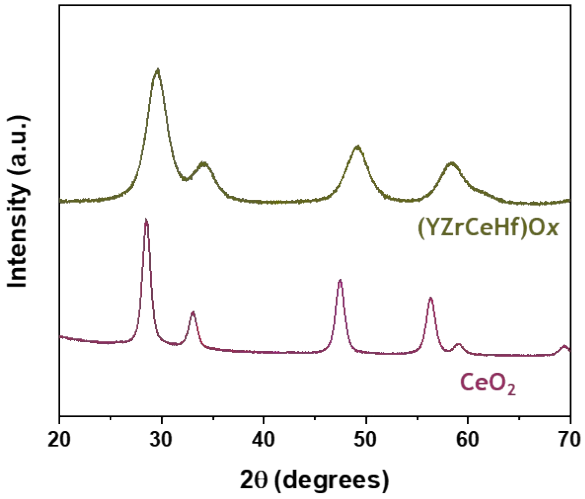

Fig. S1 | XRD patterns of (YZrCeHf)O*x* and CeO_2 aerogels. Both show a simple fluorite structure, but the peaks for (YZrCeHf)O*x* are broader and shifted toward a smaller lattice parameter.

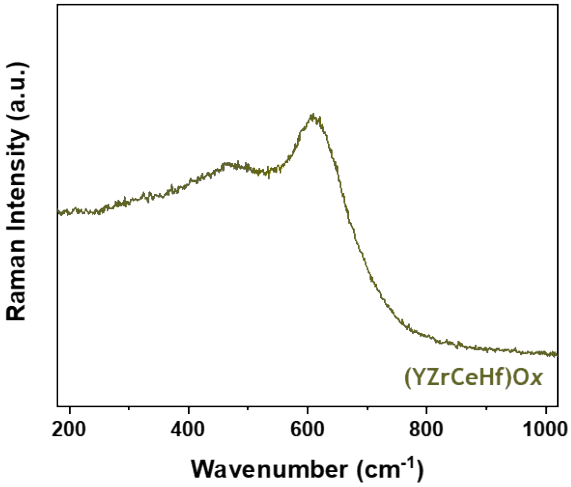

Fig. S2 | Raman spectrum of (YZrCeHf)O*x* aerogel. The broad peak at ~ 600 cm^{-1} has been assigned to oxygen vacancies previous high-entropy oxides.

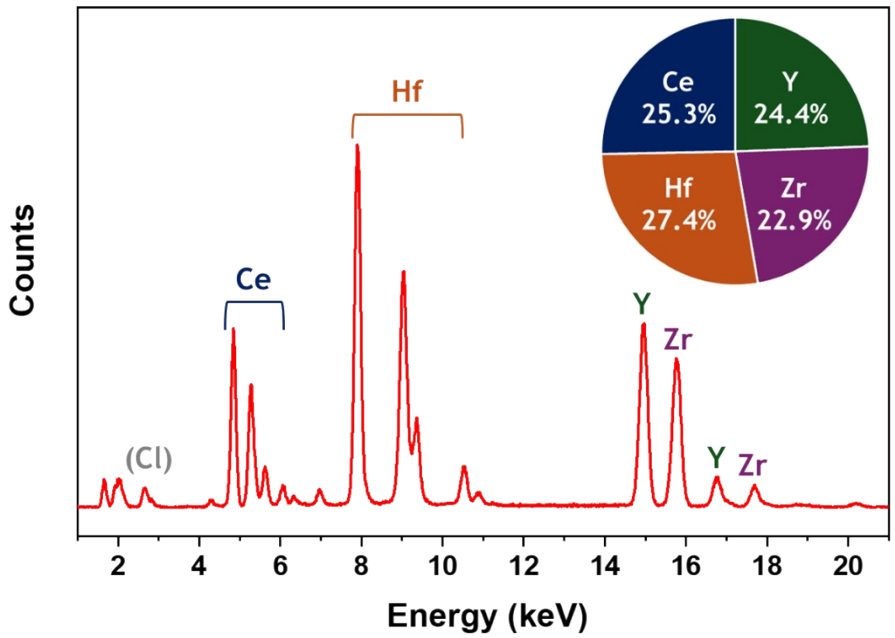

Fig. S3 | XRF-spectrum of (YZrCeHf)O*x*, with inset showing calculated elemental composition of cations. Some Cl content (~2.7 keV) is present due to the use of chloride precursors.

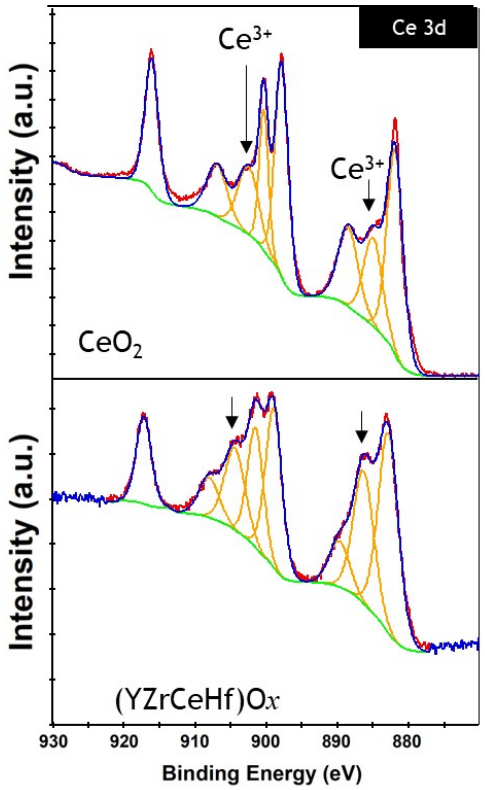

Fig. S4 | Comparison of the XPS Ce 3d region with CeO_2 and (YZrCeHf)O_x aerogels.

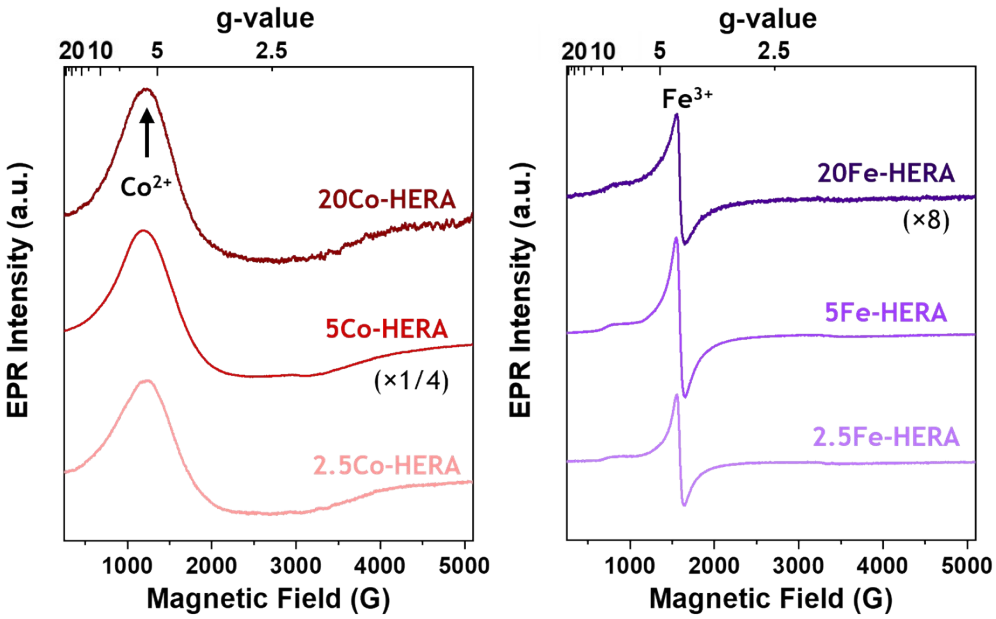

Fig. S5 | EPR of Co and Fe incorporated HERAs.

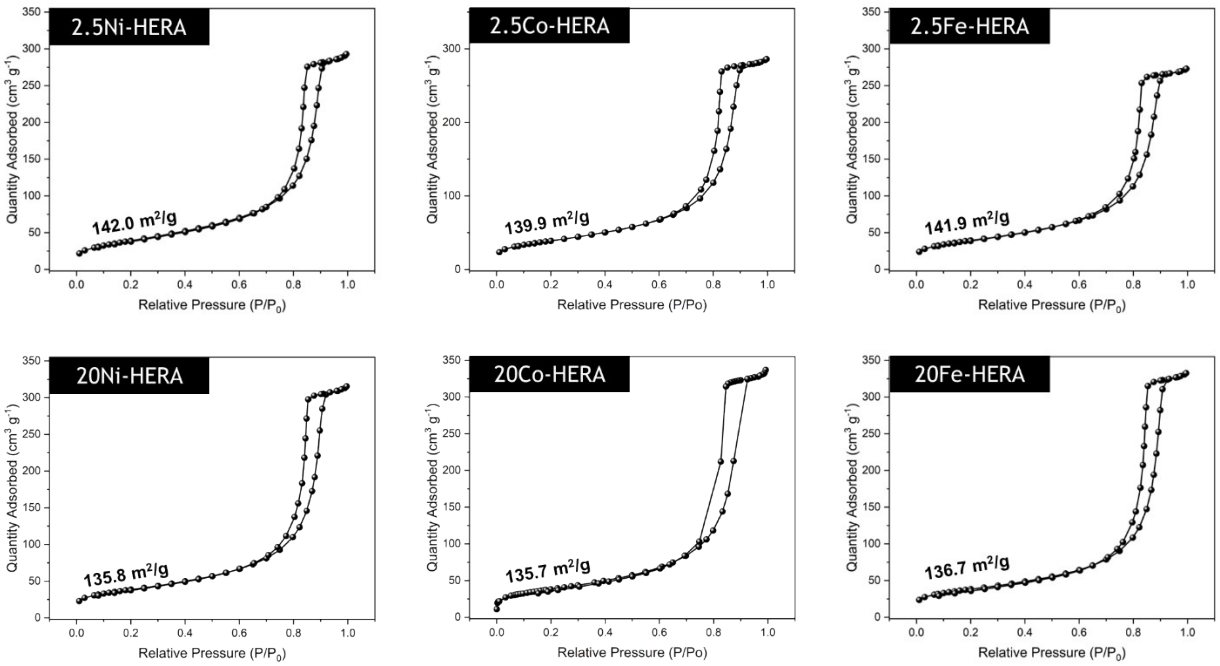

Fig. S6 | N_2 isotherms of transition-metal–incorporated HERAs, with BET surface area indicated.

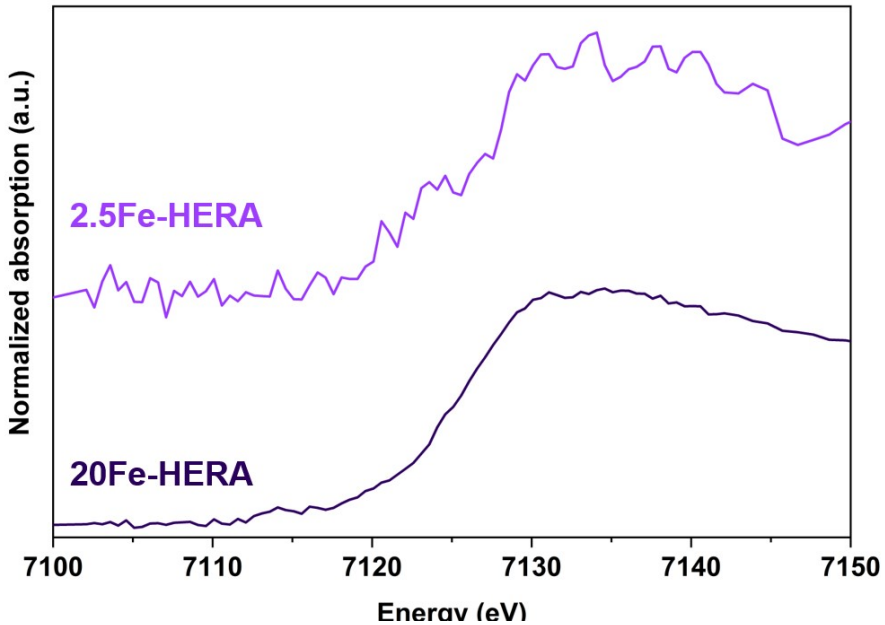

Fig. S7 | XANES comparison of 2.5Fe-HERA and 20FeHERA

Table S1 | Comparison of pre-edge peaks for standard Fe^{3+} compounds and 20Fe-HERA

Material	Centroid (eV)	Integrated Area $^{\Delta}$	Ref.
α-Fe_2O_3	7114.4	0.15	This work
α-Fe_2O_3	7114.4*	0.12	[32]
α-Fe_2O_3	7114.4	0.12	[31]
$FePO_4$	7114.5	0.32	This work
$FePO_4$	7114.5*	0.34	[32]
$FePO_4$	7114.5	0.25	[31]
20Fe-HERA	7114.1	0.12	This work

* Centroid position adjusted from primary source to account for differences in Fe foil energy calibration

$^{\Delta}$ Integrated area calculated after background subtraction and fitting the peak near 7114 eV with a single pseudo-Voigt function.

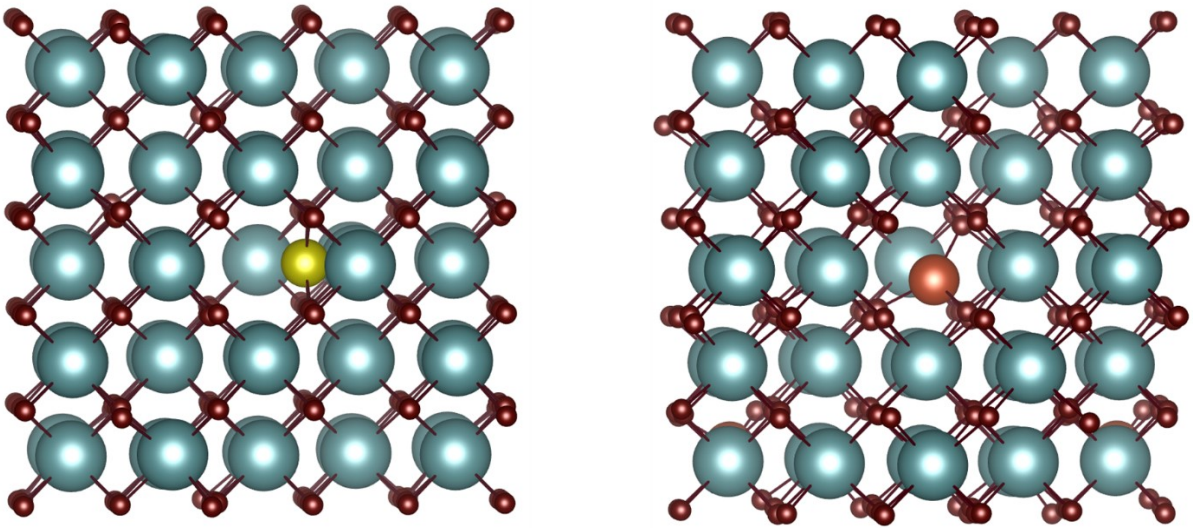

Fig. S8 | CeO_2 lattice with Ni (left) and Fe (right).

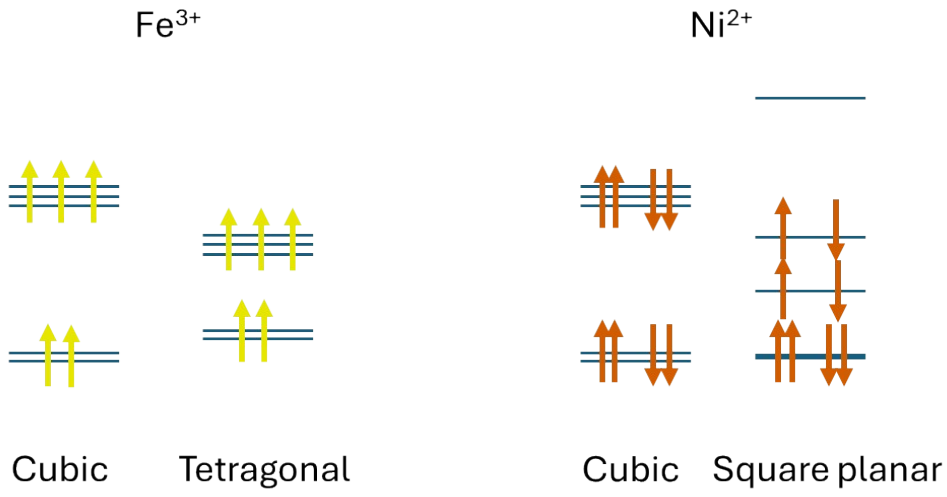

Fig. S9 | Molecular orbital diagrams for Fe^{3+} and Ni^{2+}.

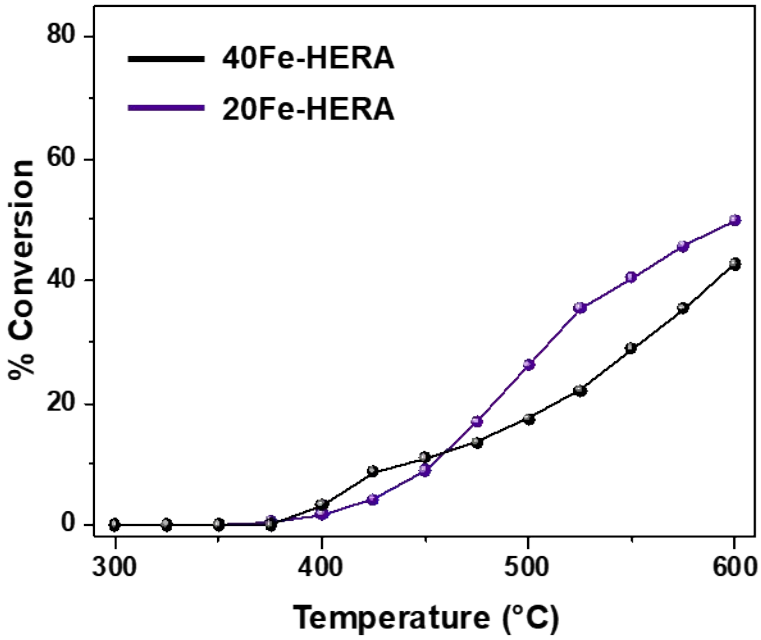

Fig. S10 | Comparison of 20 and 40 at.% Fe in HERA catalysts. Both catalysts yield entirely CO; no CH_4 is detected.

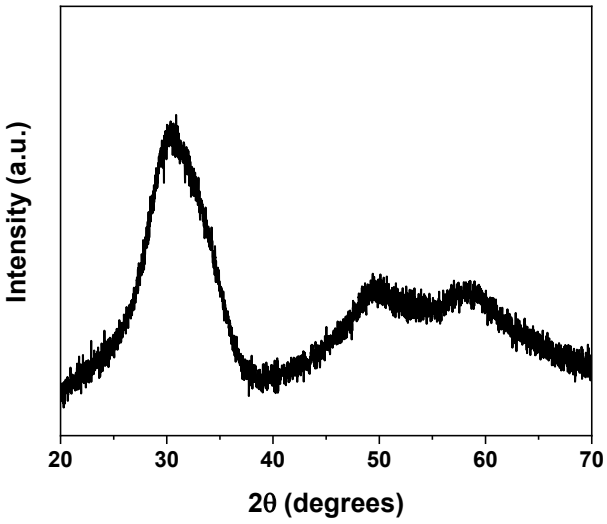

Fig. S11 | X-ray diffraction pattern of 40Fe-HERA.

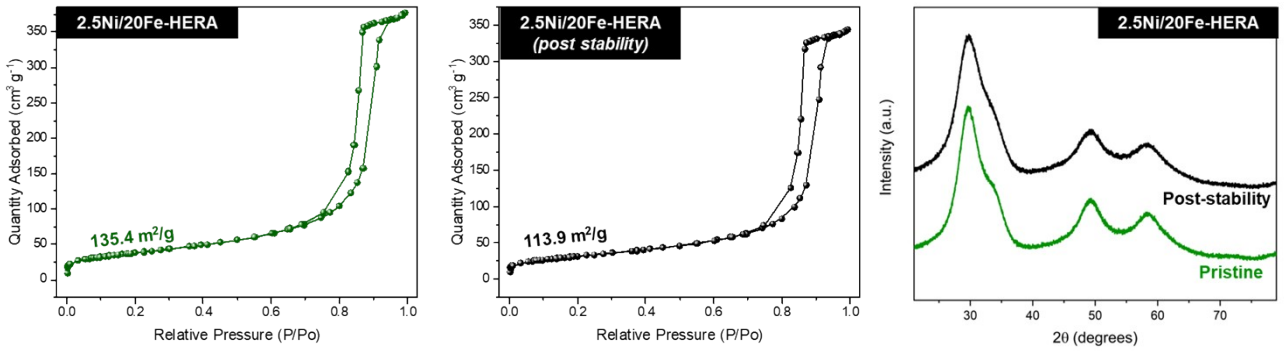

Fig. S12 | N_2 isotherms showing only slight loss of surface area loss after 90 h at 500 °C. XRD patterns remain entirely fluorite with no other phases detected.

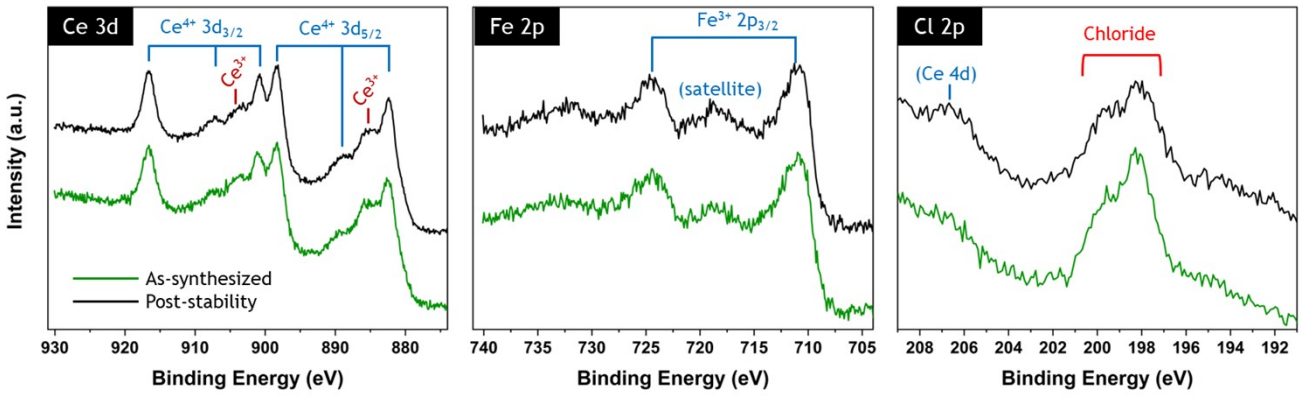

Fig. S13 | XPS high-resolution scans of the Ce 3d, Fe 2p, and Cl 2p regions of pristine and post–stability tested 2.5Ni-20Fe-HERA.

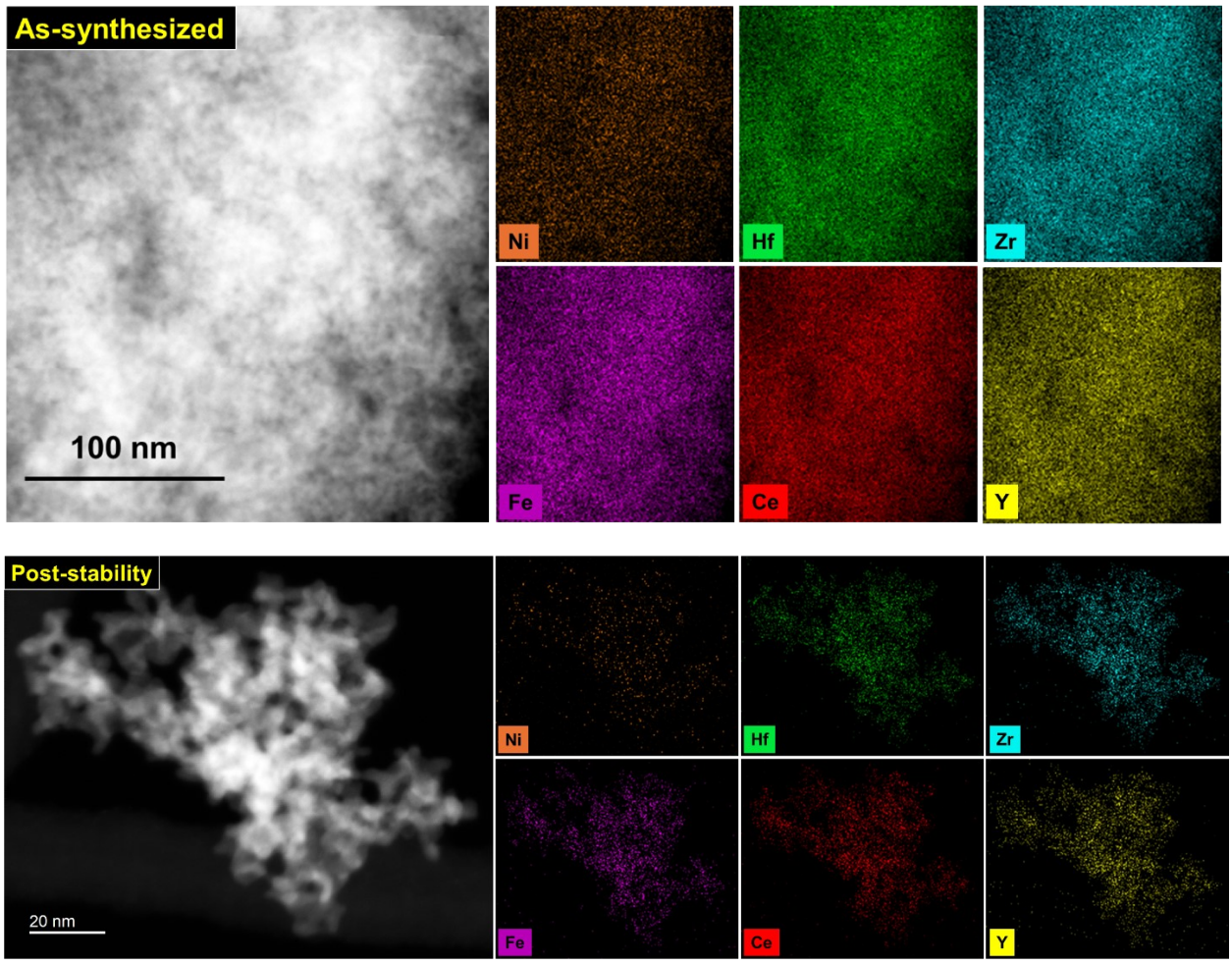

Fig. S14 | Transmission electron micrographs and EDS elemental maps of pristine (top) and post–stability test (bottom) 2.5Ni-20Fe-HERA .